3rd AIAA Flow Control Conference, 5 - 8 June 2006, San Francisco, California

A Reduced Order Galerkin Model for the Reacting Bluff Body Flame Holder

Fu Li* and Gilead Tadmor†

Communication & Digital Signal Processing Center,

Northeastern University, 440 Dana Research Building, Boston, MA 02115, U.S.A.

Bernd R. Noack‡

Hermann Föttinger-Institut für Strömungsmechanik, Sfb 557,

Technische Universität Berlin, Straße des 17. Juni, 10623 Berlin, Germany

Andrzej Banaszuk§

United Technologies Research Center, MS 129-15,

411 Silver Lane, East Hartford, CT 06108, U.S.A.

and Prashant G. Mehta¶

Mechanical and Industrial Engineering

University of Illinois at Urbana-Champaign, Urbana, IL 61801, U.S.A.

A low dimensional Galerkin model is developed for the near wake flow behind a flameholder. The model includes the two leading proper orthogonal decomposition (POD) modes, representing the first von-Kármán vortex shedding harmonic, characteristic of the non-reactive flow, and a shift mode, capturing energy balancing with a dynamic mean field correction. The model is used to demonstrate the attenuating effect of heat release on vortex shedding. In particular, vortex shedding suppression due to combustion can be explained by the emergence and the stabilizing effect of a hot shift mode, associated with expansion due to heat release.

I. Introduction

The dynamics of the premixed 2–D bluff body flameholder has been studied extensively as a geometrically simple benchmark for important applications, such as combustion instabilities in turbine and rocket engines. The non-reacting cold flow gives rise to von Kármán vortex shedding beyond a critical Reynolds number ($Re \approx 50$, varying with the specific configuration). This instability is recognized as a symmetry breaking, resulting from growth of unstable modes through Hopf bifurcation[1–3]. Both experiments and numerical simulations show that combustion leads to vortex shedding suppression and an increasingly symmetrized flow[4,5]. Yet the mechanism of transition from an asymmetric vortex shedding to a more stable and symmetric flow is not fully understood. Baroclinic vorticity generation has been suggested[5–11] as a dominant mechanism for the suppression of von Kármaán instability in the reacting flameholder. Another stabilizing factor that has been considered[5] is the increased kinematic viscosity of the reacted fluid. Yet a recent sudy[12] demonstrated

*Post-Doctoral Fellow

†Professor, CDSP Director

‡Ass. Professor

§UTRC Fellow and (acting) Control and Embedded Systems Group Leader

¶Assistent Professor

that a key stabilizing effect is rather the dilatation due to combustion heat release. That paper showed that the near wake dynamics of the reactive flameholder is dominated by the vorticity generated at the bluff body walls, while baroclinic vorticity has a significant impact on the far field vortex dynamics. In the present article we use a low dimensional model to further substantiate the role of dilatation in near wake stabilization of the reacting bluff body dynamics: We develop an extended proper orthogonal decomposition (POD) model for the premixed combustion in a single rectangular bluff body flameholder in a channel. The model captures the dynamics of dominant attractor structures in the cold and the reacting flow, as well as transients connecting such attractors. It demonstrates the stabilizing effect of a mean field *dilatation mode*, associated with combustion, in the near wake.

Since the pioneering work of[13,14], POD based low dimensional modeling has been widely applied for coherent structure analysis of turbulence and other unsteady flows. Extensive discussions and numerous references are available in[15,16]. Studies of low order models for vortex shedding behind the nonreactive bluff body have proceeded along two parallel fronts: In one direction, low dimensional models have been used to explore the dynamics of vortex shedding. On the other front, model-based control aims to design robust feedback control for the wake flow, using low order models. We can mention only few examples of the voluminous and rapidly growing literature. POD modeling of the wake flow past a circular cylinder and a grooved channel was was introduced and investigated in[17]. That seminal study showed that the asymmetric vortex shedding is well represented by the first two POD modes, and that dynamics of deviations from the attractor can be described by a six dimensional Galerkin system. An extension to the three dimensional wake is presented in[18]. A POD model based vortex shedding control, using a neutral system, was developed in[19]. Optimal and physics based control for the oscillatory rotating cylinder and the dependence of performance on model selection, were investigated, e.g., in[20–22]. Extensive numerical and experimental studies of POD based control of the vertically oscillating cylinder have been carried at the US Air Force Academy[23,24]. A POD model and model based control for a confined square cylinder were developed in[25].

A main appeal of the POD approach is its efficiency in providing high (kinematic) resolution with relatively low order models. The 95% resolution of the perturbation energy in a 2–D laminar cylinder wake flow, with a single mode pair, is a case in point[17,26]. A major drawback of this method, however, is its fragility: The associated Galerkin dynamic system tends to be highly sensitive to changes in flow conditions, such as in the Reynolds number (Re), and it is often incapable to provide ample transient representation. To alleviate these shortcomings, the authors introduced the concept of a *shift mode*[26]. The shift mode captures the stabilizing effect of the mean field correction, noted by several earlier studies[27,28]. Its inclusion in an augmented model reduces model sensitivity and is an enabler for the low dimensional representation of the transient manifold, connecting the unstable steady solution to the attractor. A series of subsequent studies investigated model calibration issues, compensating for energy flow and pressure term distortions, intrinsic to very low order Galerkin models[29,30], tuned models that improve resolution over long transients[31], the incorporation of control[32], and the use of such models in control design[29,31,33].

In the present article we demonstrate that an augmented POD model comprising the two POD modes of the leading harmonic and a shift mode, provides a good dynamic representation of both the cold and the reactive 2–D flameholder wake flows. We further show that, the mean-field correction, shift mode, changes in the reactive flow, and is then dominated by the contribution of a mode capturing the dilatation effect in the simulation model. This change results in an elevated stabilization effect in the associated Galerkin system, explaining the role of dilatation in suppressing Von Kármán vortex shedding.

The paper is organized as follows. Section **??** outlines the main features of the benchmark studied in this paper and briefly review the POD approach. The three dimensional Galerkin model for the non-reacting cold flow is presented in Section III. the bulk of the paper is occupied by Section IV, where a counterpart model is developed for the reacting flow, and the stabilizing effect of combustion, captured by the mean field correction, are demonstrated. Our numerical results and conclusions are discussed and summarize in Section 5.

II. Preliminaries

A. The flameholder and its simulation model

The configuration of a 2–D rectangular bluff body flameholder, placed in a channel, is shown in Fig. 1. The channel height is denoted H and the flameholder height is $h = 0.25H$. The origin $(0, 0)$ is placed at the midpoint of the bluff body leading edge, and the bluff body midline is coincident with the channel midline.

The horizontal incoming flow U_∞ is specified at the upstream entrance, which provides a constant influx of reactants of density ρ_u. The Mach number is assumed to be low, so both the reactants of density ρ_u and the products of density ρ_b can be treated as ideal gases. Combustion is assumed to be infinitely fast compared to the flow and a thin flame sheet model is used for the reacting flow. The two flame sheets are generated from the two front corners of the flameholder $(0, \frac{h}{2}), (0, -\frac{h}{2})$. We are investigate here the onset of the von Kármán instability, in the early wake. A short computational domain is selected accordingly

$$\Omega \doteq \{\mathbf{x} = (x, y) \, : \, x_{min} = -0.5H \leq x \leq x_{max} = 2.0H, \, -0.5H \leq y \leq 0.5H\} \subset \mathbb{R}^2. \tag{1}$$

The no-slip and impermeability boundary condition are imposed on the bluff body walls. In the simulation model used in this paper, combustion is modeled by a Lagrangian flame sheet model (the G-equation[34]) and the unsteady nonreacting and reacting flows are simulated by a Lagrangian vortex element method, where the flame sheet and the flow field are discretized over a number of elements. Details of the numerical procedure and a detailed discussion of combustion effects on flow dynamics, analyzed in terms of numerical simulations with that model, can be found in[12] .

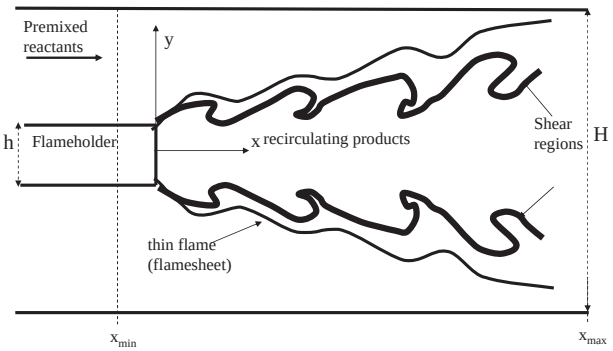

Figure 1. Problem configuration.

Combustion results in heat release and subsequently, mass volume expansion expressed as an irrotational dilatation. Following the observations that baroclinic vorticity becomes a significant factor only further downstream, the model used here includes only the dilatation effect on the reacting flow. As will be seen, vorticity generated by combustion through that process tends to suppress vortex shedding, transforming flow dynamics from the asymmetric Von Kármán vortex shedding to a more symmetric form.

B. POD Galerkin Models for the incompressible Flow

Empirical Galerkin models are based on experimental flow data or on a direct numerical simulation of the flow. The flow domain is denoted Ω (e.g., the computational domain in (1)) and velocity fields are embedded in the Hilbert space of square-integrable vector fields $\mathcal{L}_2(\Omega)$, with the inner product

$$(\mathbf{u}\,, \mathbf{v})_\Omega := \int_\Omega dV \; \mathbf{u} \cdot \mathbf{v}\,, \quad \mathbf{u}\,, \, \mathbf{v} \in \mathcal{L}_2(\Omega). \tag{2}$$

The Galerkin approximation of the flow is in the form

$$\mathbf{u}^{[N]} = \mathbf{u}_0(\mathbf{x}) + \sum_{i=1}^{N} a_i(t) \, \mathbf{u}_i(\mathbf{x}), \tag{3}$$

where $\mathbf{u}_0$ is a chosen base flow (e.g., the time-averaged field) and where $\mathbf{u}_i$, $i = 1, \ldots, N$, form an orthonormal set of Karhunen-Loève modes of the perturbations from the base flow, with respect to the inner product (2). Time dependence is restricted to the Fourier coefficients a_i. In the snapshot method[15,16] , the Karhunen-Loève modes $\mathbf{u}_i$ are constructed as linear combinations of the fluctuation snapshots $\mathbf{u}^m - \mathbf{u}_0$, $m = 1, \ldots, M$,

$M \geq N$. The chosen combinations coefficients are the top eigenvectors of the the correlation matrix of the perturbation snapshots. This selection is optimal in the sense that it minimizes the averaged energy residual of the Galerkin approximation (3), given the allowed number of modes.

A standard way to obtain a dynamical (Galerkin) system for the evolution of the Fourier coefficients is the Galerkin projection of the Galerkin ansatz (3) onto the Navier-Stokes equation, which yields a system of ordinary differential equations[15,16] .

$$\frac{d}{dt}a_i = \frac{1}{Re}\sum_{j=0}^{N} l_{ij}\, a_j + \sum_{j,k=0}^{N} q_{ijk}\, a_j\, a_k \quad \text{for } i = 1, \ldots, N, \tag{4}$$

Here the linear and quadratic terms represent the viscous and convective Navier-Stokes terms, respectively, with constant coefficients $l_{ij} := (\mathbf{u}_i, \triangle \mathbf{u}_j)_\Omega$, $q_{ijk} := (\mathbf{u}_i, \nabla \cdot (\mathbf{u}_j, \mathbf{u}_k))_\Omega$. The pressure term may change the coefficients q_{ijk}, but not the form (4)[30] . It is well known, however, that the Galerkin projection may lead to dynamic distortions, especially in very low order models[30,35] due to truncation of the energy cascade and effects of a compact computational domain. We shall therefore use parameter estimation techniques[35–37] to determine the Galerkin system coefficients.

III. Low dimensional model for vortex shedding in the nonreacting flow

Here we review a variant of the enhanced POD Galerkin model[26] of the nonreacting flow past the bluff body. The flow satisfies the continuity and the incompressible, unsteady Navier-Stokes equations

$$\nabla \cdot \mathbf{u} = 0 \tag{5}$$

$$\frac{\partial \mathbf{u}}{\partial t} + (\mathbf{u} \cdot \nabla)\mathbf{u} = -\nabla p + \frac{1}{\mathrm{Re}}\Delta \mathbf{u}, \tag{6}$$

The flow velocity in (5)-(6) is nondimensionalized by the incoming flow velocity U_∞, length, by the width of bluff body h, time, by $\frac{h}{U_\infty}$, and the pressure field p, by ρU_∞^2, where ρ is the density field. The Reynolds number is defined here, based on these normalizations $Re = \frac{U_\infty h}{\nu}$, where ν is the kinematic viscosity of the flow. Unless otherwise specified, the flow is analyzed at $Re = 1000$.

The natural attractor is dominated by von Kármán vortex shedding at period $T \approx 1.575$. To analyze the attractor in terms of its POD modes, flow snapshots were sampled at $\Delta t = 0.05$. Fig. 2 present the top ten eigenvalues of the correlation matrix of snapshot perturbations from the attractor mean. The eigenvalues represent the energy in the corresponding POD modes. As is typical to the von Kármán instability[17,26] , the

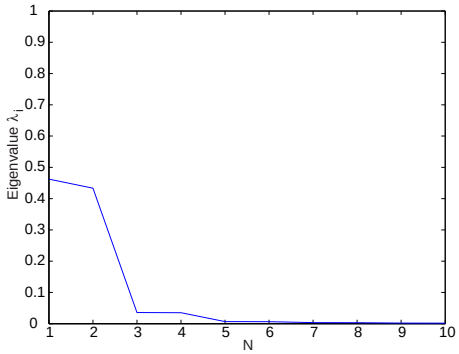

Figure 2. Cold flow: Normalized eigenvalues of the correlation matrix of snapshot perturbations.

flow is dominated by the first mode pair, $\mathbf{u}_i$, $i = 1, 2$, which is approximately anti-symmetric with respect to the horizontal equator, resolves the first vortex shedding harmonic and accounts for about 90% of the total perturbation energy. These two modes are thus sufficient to capture the dominant characteristics of the shedding instability. The next, symmetric mode pair, ($\mathbf{u}_i$, $i = 3, 4$, represent the second harmonic and account for some 6% of the perturbation energy.

It has been observed in other bluff body studies[17,26] that while POD modes lead to highly efficient Galerkin approximations of the attractor, the associated Galerkin systems (4) are fragile, and their dynamic

prediction power is, at best, limited to a small neighborhood of the attractor. The reason is that the approximation is derived, in the first place, from kinematic, rather than dynamic considerations. As a non-equilibrium model for transient flow, the authors have elaborated the need for a shift-mode in[26,33]. This shift-mode $\mathbf{u}_s$ is an orthonormalized mean-field correction. Physically, the shift mode captures the dynamics of energy balancing between an instability, such as the von-Kármán vortex shedding, and the mean flow. It therefore has a stabilizing effect and its incorporation in the model is an enabler for transient representation that includes the saturation of the instability level, on the attractor. These observations are in agreements with earlier studies, indicating the significance of mean-field corrections[27,28]. In the closely related 2–D cylinder wake flow, the shift mode was estimated as the difference between the unstable steady Navier-Stokes solution $\mathbf{u}_s$ and the time-averaged flow $\mathbf{u}_0$. Here we shall estimate the shift mode from POD analysis of transient data: Under the mean-field correction ansatz, the non-oscillatory component of transients leading to the attractor are dominated by the shift mode. We shall exploit the symmetry of the flameholder configuration, which implies both the anti-symmetric structure of the first harmonic, and the symmetry of the mean-field correction. Thus the shift mode will be extracted as the dominant symmetric and non-oscillatory flow transient component.

In all, we shall use a Galerkin approximation of the form

$$\mathbf{u}(x,t) = \mathbf{u}_0(\mathbf{x}) + \sum_{i=1}^{2} a_i(t)\mathbf{u}_i(\mathbf{x}) + a_s(t)\mathbf{u}_s(\mathbf{x}) \tag{7}$$

where $\mathbf{u}_0$ is the time-averaged mean flow, $\mathbf{u}_i$, $i = 1, 2$ are the first two POD spatial modes and $\mathbf{u}_s$ is the shift mode. Fig. 3 shows isocontour line of the first two POD modes $\mathbf{u}_i$, $i = 1, 2$, and the shift mode $\mathbf{u}_s$.

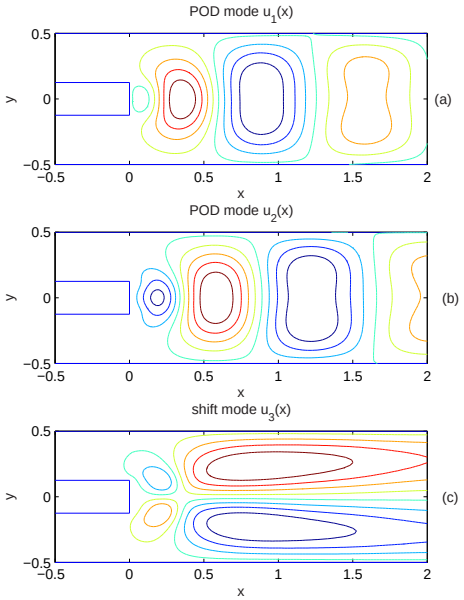

Figure 3. The POD modes $\mathbf{u}_i$, $i = 1, 2$ and the shift mode $\mathbf{u}_s$, depicted by stream function isocontours.

The structure of the phase-averaged dynamic Galerkin system of ODEs for the Fourier coefficients is derived from the Galerkin projection of the NSEs (6)

$$\frac{d}{dt}\begin{bmatrix} a_1 \\ a_2 \\ a_s \end{bmatrix} = \begin{bmatrix} 0 & -\omega - \gamma a_s & -\beta a_1 \\ \omega + \gamma a_s & 0 & -\beta a_2 \\ \alpha a_1 & \alpha a_2 & -\sigma_s \end{bmatrix} \begin{bmatrix} a_1 \\ a_2 \\ a_s \end{bmatrix} + \begin{bmatrix} 0 \\ 0 \\ g \end{bmatrix} \tag{8}$$

where $\sigma_s, \omega, \gamma, \alpha, \beta$ are all positive parameters. An equivalent system is based on the cylindrical coordinates

$a_1 = r\cos(\phi)$ and $a_2 = r\sin(\phi)$. In these terms

$$\begin{aligned} \dot{r} &= -\beta a_s\, r \\ \dot{a}_s &= -\sigma_s a_s + \alpha r^2 + g \\ \dot{\phi} &= \omega + \gamma a_s \end{aligned} \tag{9}$$

As in the case of the cylinder wake[26], this structure readily reveals key system properties: The existence of a periodic attractor, the instability of the steady solution, the stabilizing effect of the shift mode, and the dependence of the shedding period on changes in the mean flow. As noted earlier, coefficient values obtained by the Galerkin projection tend to reflect energy flow rate distortions that are intrinsic to low order Galerkin models. As in the cylinder wake model[35], we therefore obtain corrected coefficient values in (8) by *least mean squares (LMS)* matching with empirical data. Fig. 4 demonstrates a good agreement of the Fourier time series, as predicted by the estimated Galerkin system (8) and from numerical simulation of the NSE (6). In particular, the Galerkin system accurately predicts the radius of the limit cycle $r \approx 0.46$ and the attractor frequency, and a good estimate of the growth rate associated with the instability. This

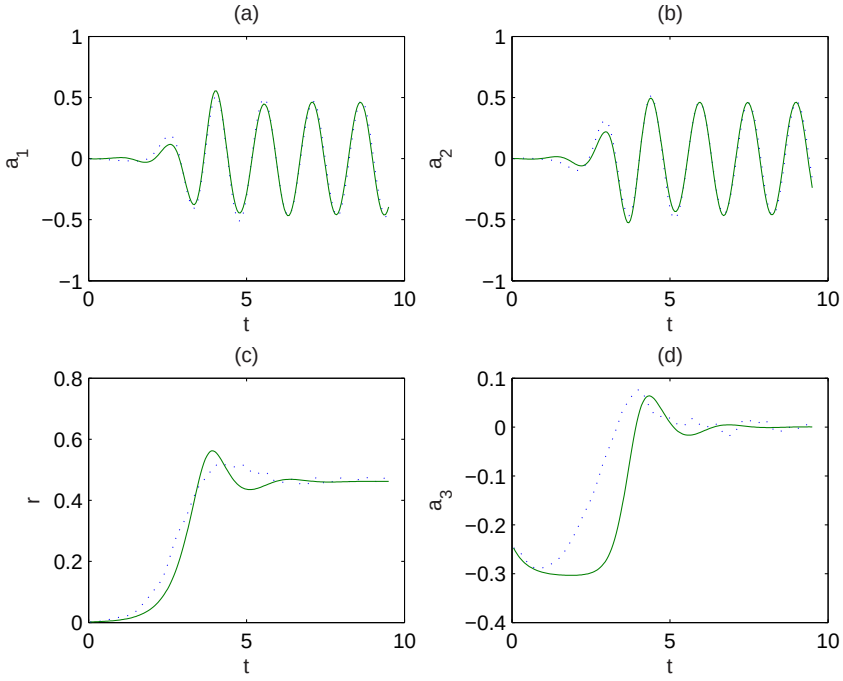

Figure 4. Cold flow: Comparison of Fourier series from low dimensional model and NS simulation. The solid line is from model, the dotted line from NS simulation. (a). $a_1(t)$**; (b).** $a_2(t)$**; (c).** $r(t) = \sqrt{a_1^2 + a_2^2}$**; (d).** $a_s(t)$**.**

comparison demonstrates the stabilizing role of the shift modes, as well as the fact that the second (and higher) harmonics have no decisive effect on the dynamics and can thus be safely neglected in a low order model.

IV. The Reacting flow model and the stabilizing effect of combustion

A. A simplified physical representation

Combustion and the inclusion of the thermodynamical process and energy evolution results with more complicated flow dynamics, including compressibility. Thus, the divergence free property (5) is no longer

satisfied. The compressible continuity and momentum equations then take the form

$$\frac{1}{\rho_k}\frac{D\rho_k}{Dt} + \nabla \cdot \mathbf{u} = 0 \tag{10}$$

$$\frac{\partial \mathbf{u}}{\partial t} + (\mathbf{u}\cdot\nabla)\mathbf{u} = -\frac{1}{\rho_k}\nabla p + \frac{1}{Re}\left[\Delta \mathbf{u} + \frac{1}{3}\nabla(\nabla\cdot\mathbf{u})\right] \tag{11}$$

where $\frac{D}{Dt}$ is the material derivative, the density is nondimensionalized with respect to the unburned mixture density ρ_u, so that $\rho_k = \frac{\rho}{\rho_u}$, and the pressure term p is nondimensionalized with respect to $\rho_u U_\infty$.

Most POD-based low dimensional models to date were derived for the simpler, incompressible flows. In a recent parting from this tradition[38], thermodynamical and velocity variables were combined in POD-based low dimensional modeling of a compressible flow. Leveraging the properties of the near wake flow under consideration, we follow[12] and maintain a focus on the velocity field variable, rather than on the thermodynamics variables, both in the simulation and in the reduced order Galerkin models. Directing the reader to[12] for details, we note here that the model is based on the approximation that, in the near wake, the flow may be roughly divided into a pre-reacted fluid region, where $\rho_k \equiv 1$, and a post combustion, reacted fluid region, where $\rho_k \equiv \frac{\rho_u}{\rho_b}$. The two regions are therefore each characterized by a fixed density, incompressible flow, separated by the flame sheets. Combustion intensity is characterized by the difference between the density of the reactant and that of the product with a nondimensional parameter $\mu = \frac{\rho_u}{\rho_b} - 1$. All other variables remain as defined earlier.

B. POD approximation

POD analysis of the attractor of the reacting reacting, hot flow, is performed in complete analogy to the non-reacting case; that is, based on velocity field snapshots and using the respective attractor mean as the base flow. We maintain our focus on the first harmonic Galerkin approximation

$$\mathbf{u}(\mathbf{x},t) = \mathbf{u}_{h0}(\mu,\mathbf{x}) + \sum_{i=1}^{2} a_i(t)\mathbf{u}_{hi}(\mu,\mathbf{x}) \tag{12}$$

where $\mathbf{u}_{h0}(\mu,\mathbf{x})$ is the mean of the reacting flow and $\mathbf{u}_{hi}(\mu,\mathbf{x})$, $i = 1,2$ are the first two POD modes of hot flow perturbations from $\mathbf{u}_{h0}$. As an example, Fig. 5 depicts the associated time trajectories of the Fourier coefficient $a_i(t)$, $i = 1,2$, for $\mu = 2.5$. The amplitude of these Fourier coefficients is significantly lower than in the nonreacting flow (depicted in Fig. 4), demonstrating the suppression of vortex shedding by combustion.

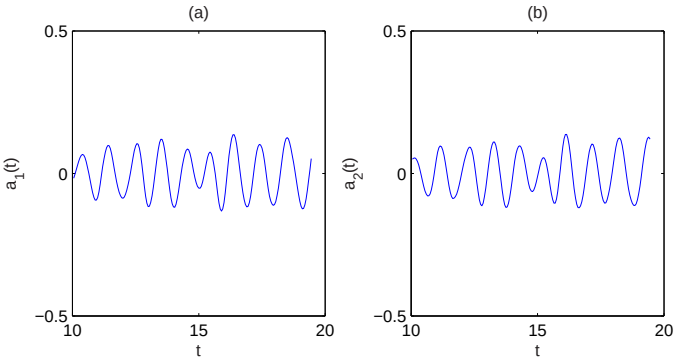

Figure 5. Hot attractor trajectories of the 1st harmonic POD Fourier coefficients $a_i(t)$, $a_2(t)$, at $\mu = 2.5$.

This POD approximation demonstrates the vortex shedding suppression phenomenon, but does not elucidate its underlying dynamic mechanism. The ensuing analysis will lead to the development of a unifying dynamic modeling framework, akin to (8). It will be valid from the low combustion level of $\mu = 0.25$, to $\mu = 2.75$, where shedding is strongly attenuated. The dynamic model will be used to reveal the direct stabilizing effects of combustion on vortex shedding dynamics. The nonreacting mean of the cold flow attractor, $\mathbf{u}_0$, will be a shared base flow, in the underlying Galerkin approximations, which as in the cold flow, will include the first vortex shedding harmonic and a mean field correction.

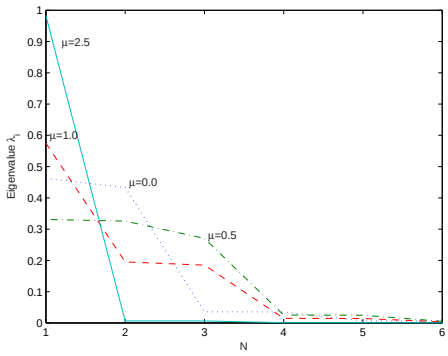

Figure 6. Eigenvalues of the correlation matrix of $\mathbf{u}(\mu, \mathbf{x}, t) - \mathbf{u}_0(\mathbf{x})$ for the reacting hot flow at different values of the combustion intensity variable μ: Cold flow, $\mu = 0.0$, dotted line; $\mu = 0.5$, dash-dotted line; $\mu = 1.0$, dashed line; $\mu = 2.5$, solid line.

Fig. 6 depicts the dominant eigenvalues of the correlation matrix of perturbations of the flow field, $\mathbf{u}(\mu, \mathbf{x}, t) - \mathbf{u}_0(\mathbf{x})$, for four values of the combustion parameter μ, ranging from the nonreacting $\mu = 0$ to $\mu = 2.5$. In considering these values it should be noted that the use of $\mathbf{u}_0$ as a joint base flow leads to the appearance of the steady mean field correction, the normalized $\mathbf{u}_0 - \mathbf{u}_{h0}$ as a POD mode associated with the steady state effect of combustion. This static mean field corection becomes dominant for larger values of μ (e.g., $\mu = 1$, in Fig. 6). The results for $\mu = 0$ have already been provided in Fig 2, showing the dominance of two leading eigenvalues, associated with the first harmonic of the asymmetric vortex shedding. The relative magnitude of the corresponding eigenvalues pair is reduced in the reacting flow. At $\mu = 1.0$, the steady mean field correction becomes the leading mode, accounting for about 60% of the perturbation energy and the two antisymmetric modes have receded into a secondary place; at $\mu = 2.5$, the steady mean field correction mode accounts for about 98% of the total perturbation from the cold mean flow.

A Galerkin approximation formalism, parameterized by the combustion parameter μ, takes the form

$$\mathbf{u}(\mu, \mathbf{x}, t) = \mathbf{u}_0(\mathbf{x}) + \sum_{i=1}^{2} a_i(t)\mathbf{u}_{hi}(\mu, \mathbf{x}) + a_{hs}(t)f(\mu)\mathbf{u}_{hs}(\mu, \mathbf{x}) \tag{13}$$

Here the *hot shift modes*, $\mathbf{u}_{hs}(\mu, \mathbf{x})$, represent the effects of combustion in both static and dynamic mean-field corrections. They are obtained from the POD analysis of the hot attractors, as described above. Equivalently, for each combustion level μ, the hot shift mode is the normalized difference between the mean of the reacting hot flow $\mathbf{u}_{h0}(\mu, \mathbf{x})$, and the mean of nonreacting cold flow, $\mathbf{u}_0(\mathbf{x})$

$$f(\mu) = ||\mathbf{u}_{h0}(\mu, \mathbf{x}) - \mathbf{u}_0(\mathbf{x})|| \quad \Leftrightarrow \quad \mathbf{u}_{hs}(\mu, \mathbf{x}) = \frac{\mathbf{u}_{h0}(\mu, \mathbf{x}) - \mathbf{u}_0(\mathbf{x})}{f(\mu)}. \tag{14}$$

Here $f(\mu)$ is the average mean field correction norm over the μ-attractor. Under the normalization of a_{hs} in (13), the average attractor value of a_{hs} is one, for all μ.

It is implied by the system geometry that the velocity field $\mathbf{u}_i(\mathbf{x})$, $i = 1, 2$, are antisymmetric and the mean field correction $\mathbf{u}_{hs}(\mu, \mathbf{x})$ is symmetric. Thus, these three modes form an orthonormal system. It is also noted that the change in the symmetric base flow from (12) to (13) will have no bearings on the antisymmetric $\mathbf{u}_{hi}(\mu, \mathbf{x})$, which are therefore identical in the two expressions. In Sections C and D we shall show that a reasonable model can be obtained with μ-independent modes, enabling the sought unified model and unified analysis of the effect of combustion on the von Kármán instability.

In closing this section we examine the normalizing function $f(\mu)$, as plotted in Fig. 7. The value $f(\mu)$ is a measure of the mean field change of the reacting hot flow from the nonreacting cold flow. Recalling that the shift mode captures energy exchange between the mean field and instability, it is worth noting that the value of $f(\mu)$ at higher values of μ exceeds the cold attractor's amplitude. This indicates the energetic contribution of combustion, in accelerating the near wake fluid. More significantly for the objective of this paper, the mean field correction has a stabilizing effect in models of the form of (8). Once (8) is extended, to cover the reactive flow, higher values of $f(\mu)$ will have an increasingly stabilizing effect on the attractor, providing a dynamic model for this phenomenon.

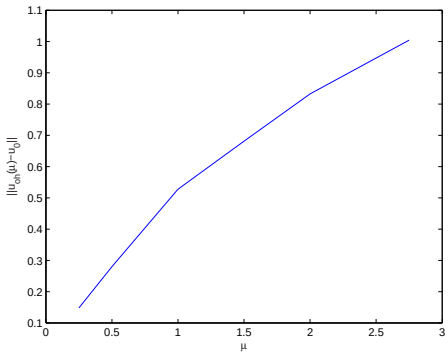

Figure 7. A plot of $f(\mu)$.

C. The hot shift mode

The impact of the combustion level μ on the orientation of the hot shift mode $\mathbf{u}_{hs}(\mu, \mathbf{x})$ is naturally assessed in terms of the function space angle between these modes, for various values of μ. Equivalently, it is evaluated in terms of the respective $\mathcal{L}_2(\Omega)$ inner products $(\mathbf{u}_{hs}(\mu_1, \mathbf{x}), \mathbf{u}_{hs}(\mu_2, \mathbf{x}))_\Omega$. Over the range of $\mu \in [0.25, 2.75]$, these inner products ranged within the interval $[0.986, 1]$, revealing a very small effect of μ on the hot shift mode. As an illustration, Fig. 8, depicts trajectories of the hot shift mode Fourier coefficient for the attractor at $\mu = 2.75$, when shift modes for various values of μ are used to compute the Fourier coefficient $a_{hs}(t) = (\mathbf{u}(\mathbf{x}, t), \mathbf{u}_{hs}(\mu, \mathbf{x}))_\Omega / f(2.75)$ Fu: IS THIS CORRECT?. As seen, the selection of the particular shift mode has little effect. The practical conclusion is that a single hot shift mode can be used in (13).

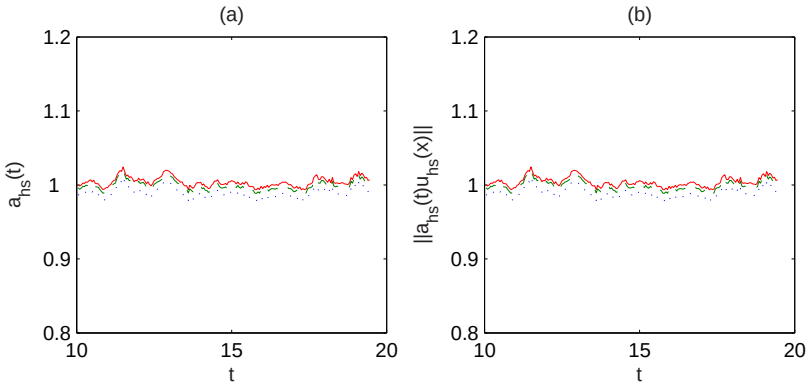

Figure 8. Comparison of $a_{hs}(t)$ and $||a_{hs}(t)u_{hs}(\mathbf{x})||$ using three different hot shift mode $u_{hs}(\mu, \mathbf{x})$ for a reacting hot flow of $\mu = 2.75$. (a). $a_{hs}(t)$; (b). $||a_{hs}(t)u_{hs}(\mathbf{x})||$. dotted line when using $u_{hs}(1.0, x)$; dashed line when using $u_{hs}(2.0, x)$; solid line when using $u_{hs}(2.5, x)$;

To understand the structure of the mean field correction and its near μ-independence, we consider the contributions of two obvious candidates: The dynamic, cold shift mode $\mathbf{u}_s$, and the velocity field associated with the volumetric expansion due to heat release. We denote the latter by $\mathbf{u}_d(\mu, \mathbf{x})$ and note that it is characterized[12] in terms of the mass conservation equation $\frac{1}{\rho}\frac{D\rho}{Dt} + \nabla \cdot \mathbf{u}_d(\mu, \mathbf{x}) = 0$. It has been established[39] that under the shallow flame angle assumption, valid here, the expansion velocity can be approximated by a linear solution

PLEASE PROVIDE FORMULA IF POSSIBLE (15)

This velocity field is normalized, to obtain an *expansion mode*:

$$\mathbf{u}_e(\mathbf{x}) = \mathbf{u}_d(\mu, \mathbf{x})/s(\mu), \qquad s(\mu) = ||\mathbf{u}_d(\mu, \mathbf{x})||.$$

The linear dependence of $\mathbf{u}_d(\mu, \mathbf{x})$ on μ means that the expansion mode is independent of μ.

Exploring the approximation of the hot sift modes $\mathbf{u}_{hs}(\mu, \mathbf{x})$ in terms of the cold shift mode $\mathbf{u}_s(\mathbf{x})$ and

the expansion $\mathbf{u}_e(\mathbf{x})$, we solve the *least mean squares (LMS)* approximation

$$\min_{\eta_e,\,\eta_s} \|\mathbf{u}_{hs}(\mu,\mathbf{x}) - \eta_e \mathbf{u}_e(\mathbf{x}) - \eta_s \mathbf{u}_s(\mathbf{x})\|. \tag{16}$$

Table 1 shows the optimal values of η_e, η_s and the corresponding norm residual, $err = ||\mathbf{u}_{hs}(\mu,\mathbf{x}) - \eta_e \mathbf{u}_e(\mathbf{x}) - \eta_s \mathbf{u}_3(\mathbf{x})||$, for $\mu \in [0.25, 2.75]$. The table reveals three basic facts: (i) The approximation in (16) leads to less than a 2% norm error (less than 13% error in energy content). (ii) The hot shift mode $\mathbf{u}_{hs}(\mu,\mathbf{x})$ is dominated by the contribution of the μ-independent expansion mode $\mathbf{u}_e(\mathbf{x})$, explaining its near independence of μ. (iii) Nonetheless, the hot shift mode contains a meaningful contribution – up to 33% of its perturbation energy – from the cold shift mode, representing nonreacting fluid dynamics.

	a	b	err
$\mu = 0.25$	0.985	0.113	0.0159
$\mu = 0.5$	0.985	0.113	0.0173
$\mu = 1.0$	0.988	0.080	0.0171
$\mu = 1.5$	0.979	0.148	0.0203
$\mu = 2.0$	0.980	0.146	0.0172
$\mu = 2.5$	0.975	0.176	0.0160
$\mu = 2.75$	0.977	0.160	0.0166

Table 1. Result of a, b and corresponding error for different μ of expression (16). $err = ||\mathbf{u}_{hs}(\mu,\mathbf{x}) - a\mathbf{u}_e(\mathbf{x}) - b\mathbf{u}_3(\mathbf{x})||$.

D. The hot first harmonic modes

Here we explore the sensitivity of the POD modes $\mathbf{u}_{hi}(\mu,\mathbf{x})$, $i = 1, 2$, to changes in the combustion intensity parameter μ, over the studied range. To begin with, we consider the correlation matrix of the entire family $\{\mathbf{u}_{hi}(\mu_k,\mathbf{x})\}_{i=1,2,k=1,\ldots,7}$ where the seven values μ_k are those used in Table 1. Fig. 9 depicts the first eight eigenvalues for this matrix, normalized by the eigenvalues' sum. It reveals that two leading eigenvalues represent about 90% of the total variation. This indicates that the collection of all first harmonic POD modes is well represented by a single mode pair.

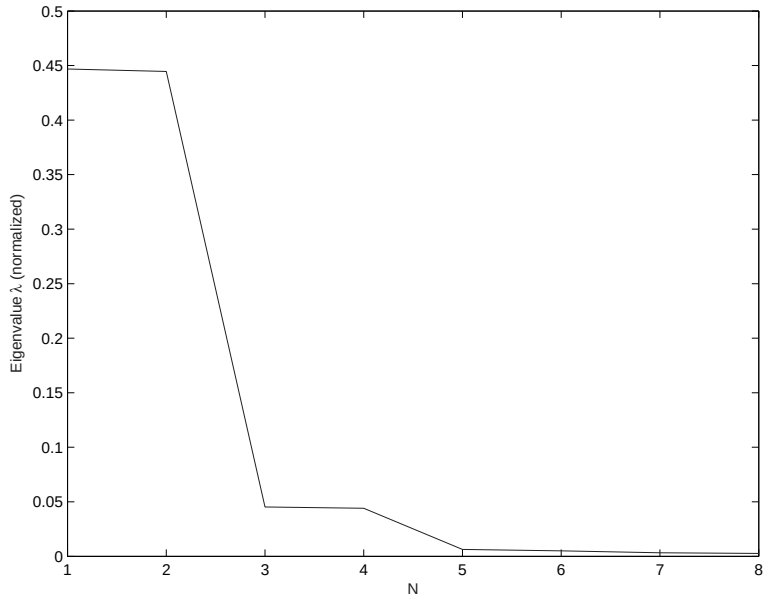

Figure 9. Eigenvalues or correlation matrix of POD modes u_1, u_2 of reacting flow for different μ.

As a matter of convenience for the comparison of the subsequent dynamic models with the cold flow model, we prefer to use the cold POD modes. To justify this selection, we also analyzed the 4×4 correlation matrices of the subsets $\{\mathbf{u}_i(\mathbf{x}), \mathbf{u}_{hi}(\mu_k, \mathbf{x})\}_{i=1,2}$, separately, for each μ_k. The resulting eigenvalues of these matrices are listed in Table 2. As seen, each of these matrices is strongly dominate by a single eigenvalues pair, with relatively small variations, even as μ reaches the value of 2.75. In particular, in each case, projection on the subspace spanned by the dominant POD modes pair of the nonreacting flow, $\mathbf{u}_i(\mathbf{x})$, $i = 1, 2$, should provide an ample representation of the instability.

	$\mu = 0.25$	$\mu = 0.5$	$\mu = 1.0$	$\mu = 1.5$	$\mu = 2.0$	$\mu = 2.5$	$\mu = 2.75$
λ_1	0.499092	0.495032	0.486292	0.482048	0.473297	0.444828	0.422224
λ_2	0.498649	0.493511	0.485422	0.481412	0.471348	0.442925	0.420439
λ_3	0.001350	0.006488	0.014577	0.018587	0.028651	0.057074	0.079560
λ_4	0.000907	0.004967	0.013707	0.017951	0.026702	0.055171	0.077775

Table 2. The first four eigenvalues for correlation matrix of hot POD modes with different μ.

E. The reduced order Galerkin system for the reacting flow

Following the conclusions, above, the Galerkin approximation (13) is replaced by an approximation in terms μ-independent modes

$$\mathbf{u}(\mu, x, t) = \mathbf{u}_0(\mathbf{x}) + \sum_{i=1}^{2} a_i(t)\mathbf{u}_i(\mathbf{x}) + a_{hs}(t)f(\mu)\mathbf{u}_{hs}(\mathbf{x}). \tag{17}$$

The Galerkin projection would, ideally, produce a system of ordinary equations for the time evolution of the Fourier coefficients $a_i(t)$ and $a_{hs}(t)$. The contribution of the combustion intensity parameter μ, in such a system, would be via the function $f(\mu)$. In compact form, the Galerkin system would be a variant of (8), where added diagonal terms account for the fact that the base flow is no more the attractor mean.

$$\frac{d}{dt}\begin{bmatrix} a_1 \\ a_2 \\ a_{hs} \end{bmatrix} = \begin{bmatrix} \beta(\mu) & -\omega(\mu) - \gamma a_{hs} & -\beta(\mu)a_1 \\ \omega(\mu) + \gamma a_{hs} & \sigma_r(\mu) & -\beta(\mu)a_2 \\ \alpha(\mu)a_1 & \alpha(\mu)a_2 & -\sigma_{hs}(\mu) \end{bmatrix} \begin{bmatrix} a_1 \\ a_2 \\ a_{hs} \end{bmatrix} + \begin{bmatrix} 0 \\ 0 \\ g(\mu] \end{bmatrix} \tag{18}$$

and its cylindrical coordinates counterpart

$$\begin{aligned} \dot{r} &= (\sigma_r(\mu) - \beta(\mu)a_{hs})\, r \\ \dot{a}_s &= -\sigma_{hs}(\mu)a_{hs} + \alpha(\mu)r^2 + g(\mu) \\ \dot{\phi} &= \omega(\mu) + \gamma(\mu)a_{hs} \end{aligned} \tag{19}$$

The convention that $a_{hs} \approx 1$ on each of the hot attractors – as opposed to $a_s \approx 0$, intrinsic in the cold flow model (18) – readily implies that here $\sigma_r(\mu) = \beta(\mu)$. The attractor size is determined by

$$r_{ha}(\mu) = \sqrt{(\sigma_{hs}(\mu) - g(\mu))/\alpha(\mu)} \tag{20}$$

Using the transient flow from cold flow to hot flow $\mu = 2.5$, we can obtain the three dimensional system for hot flow $\mu = 2.5$. Fig. 10 shows the comparison of Fourier coefficient between three mode model and Navier-Stokes simulation for this transient leading to reacting flow $\mu = 2.5$. Similarly, using the transient flow from cold flow to hot flow $\mu = 2.75$, we can obtain the system for reacting flow $\mu = 2.75$. Fig. 11 shows the comparison of Fourier coefficient between our three dimensional model and NS simulation for reacting flow $\mu = 2.75$. When μ is increased from $\mu = 0.0$ to $\mu = 2.75$, σ_r is increasing, σ_{hs} is decreasing and they have destabilizing effect on the system; However, g and α is increasing and thus stabilize the system.

References

[1]B. Ahlborn, M. Lefrançois, and D. King. The clockwork of vortex shedding. *Phys. Essays*, 11(1):144–154, 1998.

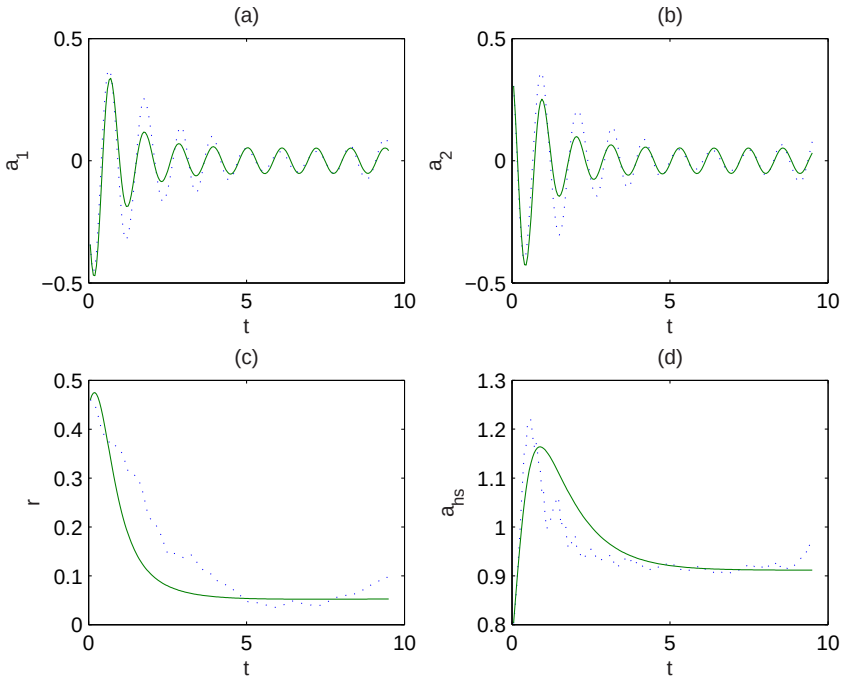

Figure 10. Comparison of Fourier series from low dimensional model and NS simulation for reacting hot flow $\mu = 2.5$. The solid line is from model, the dotted line from NS simulation. (a). $a_1(t)$; (b). $a_2(t)$; (c). $r(t) = \sqrt{a_1^2 + a_2^2}$; (d). $a_{hs}(t)$.

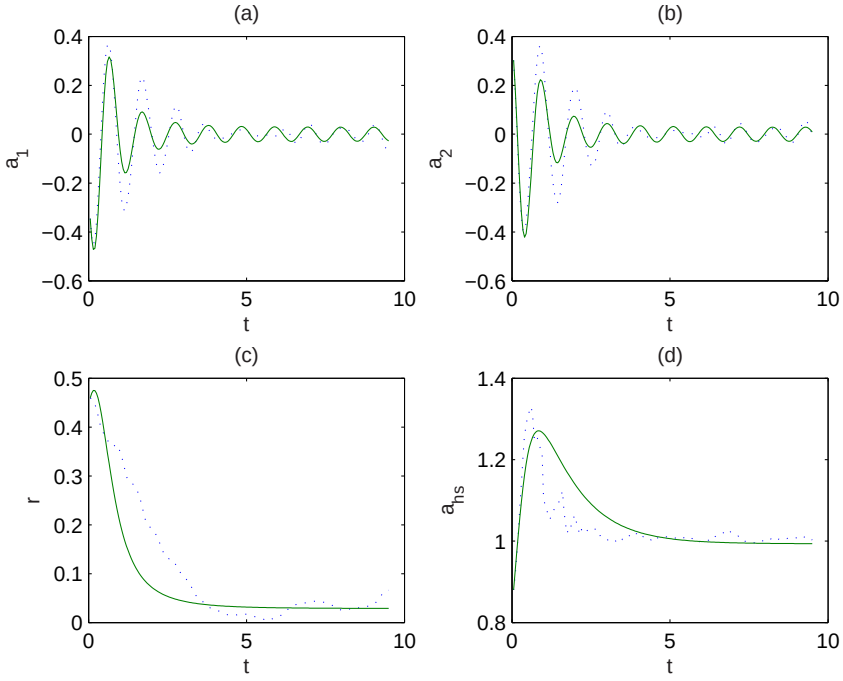

Figure 11. Comparison of Fourier series from low dimensional model and NS simulation for reacting hot flow $\mu = 2.75$. The solid line is from model, the dotted line from NS simulation. (a). $a_1(t)$; (b). $a_2(t)$; (c). $r(t) = \sqrt{a_1^2 + a_2^2}$; (d). $a_{hs}(t)$.

[2]M. Provansal, C. Mathis, and L. Boyer. Bénard-von Kármán instability: transient and forced regimes. *J. Fluid Mech.*, 182:1–22, 1987.

[3]C.Williamson. Vortex dynamics in the cylider wake. *Annu. Rev. Fluid Mech.*, 28:477–539, 1996.

[4]J.R.Hertzberg, M.Namazian, and L.Talbot. Vortex shedding behind rod-stabilized flames. *Combustion and Flame*, 86:1–11, 1991.

[5]C.M.Coats. Coherent structure in combustion. *Prog. Energy Comb. Sci.*, 22:427–509, 1996.

[6]V.K. Chakravarthy and S. Menon. Large eddy simulations of bluff body stabilized flames. In *3rd ASME/JSME Joint Fluids Engineering Conference*, 1999.

[7]A.F. Ghoniem and A. Krishnan. Origin and manifesttation of flow-combustion interactions in a premixed shear layer. In *22nd Symposium (International) on Combustion, The Combustion Institute*, pages 665 – 675, 1988.

[8]M.Z. Pindera and L. Talbot. Some fluid dynamic considerations in the modeling of flames. *Combustion and Flame*, 73:111 – 125, 1988.

[9]C.W. Rhee, L. Talbot, and J. Sethian. Dynamic behavior of premixed turbulent V-flame. *Journal of Fluid Mechanics*, 300:87 – 115, 1995.

[10]M.C. Soteriou and A.F. Ghoniem. The vorticity dynamics of an exothermic spatially developing forced, reacting shear layer. In *25th Symposium. (International) on Combustion, The Combustion Institute*, 1994.

[11]A.F. Ghoniem, A.J. Chorin, and A.K. Oppenheim. Numerical modeling of turbulent flow in a combustion channel. *Phil. Trans. R. Soc. Lond., A*, 304:303 – 325, 1982.

[12]P. Mehta and M. Soteriou. Wake dynamics of bluffbody stabilized premixed combustion - effects of exothermicity and forcing. In *41st AIAA Aerospace Sciences Meeting and Exhibit*, 2003. Paper 2003-835.

[13]L. Sirovich. Turbulence and the dynamics of coherent structures, parts i-iii. *Quarterly of Applied Mathematics*, 45 (3):561–590, 1987.

[14]N. Aubry, P. Holmes, J.L. Lumley, and E. Stone. The dynamics of chorent structures in the wall region of a turbulent boundary layer. *J. Fluid Mech.*, 192:115–173, 1988.

[15]P. Holmes, J.L. Lumley, and G. Berkooz. *Turbulence, Coherent Structures, Dynamical Systems and Symmetry*. Cambridge University Press, Cambridge, 1998.

[16]T.R. Smith, J. Moehlis, and P. Holmes. Low-dimensional models for turbulent plane couette flow in a minimal flow unit. *Journal of Fluid Mechanics*, 538:71–110, 2005.

[17]A.E. Deane, I.G. Kevrekidis, G.E. Karniadakis, and S.A. Orszag. Low-dimensional models for complex geometry flows: Application to grooved channels and circular cylinders. *Phys. Fluids A*, 3(10):2337–2354, 1991.

[18]X. Ma and G.E. Karniadakis. A low-dimensional model for simulating three-dimensional cylinder flow. *J. Fluid Mech.*, 458:181–190, 2002.

[19]E. A. Gillies. Low-dimensional control of the cylinder wake. *Journal of Fluid Mechanics*, 371:157–178, 1998.

[20]W.R. Graham, J. Peraire, and K.Y. Tang. Optimal control of vortex shedding using low-order models, Part 1: Open-loop model development, and Part 2: Model-based control. *International Journal For Numerical Methods in Engineering*, 44:945–990, 1999.

[21]B Protas and J.E. Wesfreid. Drag force in the open-loop control of the cylinder wake in the laminar regime. *Physics of Fluids*, 14:810 – 826, 2002.

[22]M. Bergmann, L. Cordier, and J.-P. Brancher. Optimal rotary control of the cylinder wake using POD reduced order model. In *2nd AIAA Flow Control Conference*, Portland, Oregon, U.S.A., 28.6.–1.7.2004, 2004. Paper 2004-2323.

[23]S. Siegel, K. Cohen, and T. McLaughlin. Feedback control of a circular cylinder wake in experiment and simulation. In *33rd AIAA Fluids Conference and Exhibit*, Orlando, Florida, U.S.A., June 23–26, 2003, 2003. Paper No 2003-3571.

[24]K. Cohen, S. Siegel, M. Luchtenburg, T. McLaughlin, and A. Seifert. Sensor placement for closed-loop flow control of a 'D' shaped cylinder wake. In *2nd AIAA Flow Control Conference*, Portland, Oregon, U.S.A., 28.6.–1.7.2004, 2004. Paper 2004-2523.

[25]B. Galletti, C.H. Bruneau, L. Zannetti, and A. Iollo. Low-order modelling of laminar flow regimes past a confined square cylinder. *Journal of Fluid Mechanics*, 503:161–170, 2004.

[26]B.R. Noack, K. Afanasiev, M. Morzyński, G. Tadmor, and F. Thiele. A hierarchy of low-dimensional models for the transient and post-transient cylinder wake. *J. Fluid Mech.*, 497:335–363, 2003.

[27]J.T. Stuart. On the non-linear mechanics of hydrodynamic stability. *J. Fluid Mech.*, 4:1–21, 1958.

[28]BJA Zielinska, S GoujonDurand, J Dusek, and J.E. Wesfreid. Strongly nonlinear effect in unstable wakes. *Physical Rev. Letters*, 79:3893 – 3896, 1997.

[29]G. Tadmor, B.R. Noack, M. Morzyński, and S. Siegel. Low-dimensional models for feedback flow control. Part II: Controller design and dynamic estimation. In *2nd AIAA Flow Control Conference*, Portland, Oregon, U.S.A., June 28 – July 1, 2004. AIAA Paper 2004-2409 (invited contribution).

[30]B.R. Noack, P. Papas, and P.A. Monkewitz. The need for a pressure-term representation in empirical Galerkin models of incompressible shear flows. *J. Fluid Mech.*, 523:339–365, 2005.

[31]O. Lehmann, M. Luchtenburg, B.R. Noack, R. King, M. Morzynski, and G. Tadmor. Wake stabilization using POD Galerkin models with interpolated modes. In *44th IEEE Conference on Decision and Control and European Control Conference ECC, Seville, Spain*, 12.-15. December 2005. (submitted).

[32]B.R. Noack, G. Tadmor, and M. Morzyński. Low-dimensional models for feedback flow control. Part I: Empirical Galerkin models. In *2nd AIAA Flow Control Conference*, Portland, Oregon, U.S.A., June 28 – July 1, 2004. AIAA Paper 2004-2408 (invited contribution).

[33]J. Gerhard, M. Pastoor, R. King, B.R. Noack, A. Dillmann, M. Morzyński, and G. Tadmor. Model-based control of vortex shedding using low-dimensional Galerkin models. In *33rd AIAA Fluids Conference and Exhibit*, Orlando, Florida, U.S.A., June 23–26, 2003, 2003. Paper 2003-4262.

[34]A. R. Kerstein, W. Ashurst, and F. A. Williams. Field equations for interface propagation in an unsteady homogeneous flow field. *Phys. Rev. A*, 37:2728 – 2731, 1988.

[35]G. Tadmor and B.R. Noack. Dynamic estimation for reduced Galerkin models of fluid flows. In *The 2004 American Control Conference*, Boston, MA, U.S.A., June 30–July 2, 2004, 2004. Paper **WeM18.1**.

[36]S. H. Jeong and B. Bienkiewicz. Application of autoregressive modeling in proper orthogonal decomposition of builing wind pressure. *J. Wind Engineering and Industrial Aerodynamics*, 69-71:685–695, 1997.

[37]S. Park, A. Wachsman, T. Yi, D. Wee, A. M. Annaswamy, and A. F. Ghoniem. A backward-facing step combustor: reduced-order modeling and control. In *IEEE Conference on Decision and Control, Maui, Hawaii*, December 9 - 12, 2003.

[38]C.W. Rowley, T. Colonius, and R.M. Murray. Model reduction for compressible flows using pod and galerkin projection. *Physica D*, 189:115–129, 2004.

[39]P.G. Mehta, M.C. Soteriou, and A. Banaszuk. Impact of exothermicity on steady and linearized response of a premixed ducted flame. *Combustion and Flame*, 141:392–405, 2005.

[40]B.R. Noack, P. Papas, and P.A. Monkewitz. The need for a pressure-term representation in empirical galerkin models of imcompressible shear flows. *Journal of Fluid Mechanics*, 523:339–365, 2005.

[41]G. Tadmor, B.R. Noack, M. Morzynski, and S. Siegel. Low-dimensional models for feedback flow control. part ii: Control design and dynamic estimation. *AIAA*, 2004-2409.